2024 IEEE Ultrasonics, Ferroelectrics, and Frequency Control Joint Symposium (UFFC-JS) | 979-8-3503-7190-1/24/$31.00 ©2024 IEEE | DOI: 10.1109/UFFC-JS60046.2024.10794118

Impact of Photoacoustic Source Location on Flexible Array Curvature Estimation with a Maximum Lag-One Spatial Coherence Metric

Jiaxin Zhang*, Kai Ding†, and Muyinatu A. Lediju Bell*‡§
*Department of Electrical and Computer Engineering, Johns Hopkins University, Baltimore, MD
†Department of Radiation Oncology and Molecular Radiation Sciences, Johns Hopkins Medical Institutes, Baltimore, MD
‡Department of Biomedical Engineering, Johns Hopkins University, Baltimore, MD
§Department of Computer Science, Johns Hopkins University, Baltimore, MD

***Abstract*—One key component to accurate photoacoustic image reconstruction with flexible array transducers is knowledge of element positions as the flexible array shape varies. Our previously proposed metric calculates the maximum lag-one spatial coherence (mLOC) of a photoacoustic target, with demonstrated advantages to estimate the curvature of a flexible array. However, the effectiveness of mLOC in relation to target locations remained unclear. Therefore, we investigated mLOC performance across different source locations by first designing a radial grid consisting of 20 simulated photoacoustic sources at varying azimuthal angles and depths. The accuracy of the mLOC-estimated array radius was 97.59%-100% when compared with the ground truth curvature. Signals from deeper sources produced greater coherence when beamforming images with the correctly estimated array radius. In addition, we introduced a normalized full-width at half-prominence (nFWHP) metric to assess the flatness of the mLOC measurements as a function of estimated array radius, demonstrating greater mLOC effectiveness with estimating flexible array radii with decreasing distance between the source and the transducer center. Therefore, the photoacoustic source should be placed as close to the array radius center as possible to achieve the best array shape estimation results with mLOC.**

***Index Terms*—flexible array shape estimation, spatial coherence**

I. Introduction

The flexibility of ultrasound transducer arrays to receive signals when configured into different shapes that conform to various body parts is an emerging area of research and development for photoacoustic imaging applications [1]–[4]. By conforming to different surfaces, complete contact between the flexible array and the surface reduces air gaps, which avoids image artifacts due to acoustic impedance mismatches [5]. In addition, compared to traditional rigid transducers which require applied pressure during data collection [6], the flexibility of a flexible array transducer mitigates patient discomfort as extra pressure is not needed to maintain acoustic coupling. Minimizing or eliminating this pressure also decreases the possibilities of organ distortion and target displacement during interventional procedures.

However, it is challenging to obtain accurate flexible array geometries when element positions change as the transducer conforms to various surfaces. Incorporating incorrect array shapes when beamforming resulting images can lead to distorted target shapes and blurred target edges [7]. To obtain correct element positions, previous work proposed to attach external sensors to the flexible array such as a shape sensing fiber [8], a strain sensor [9], and optical markers paired with an infrared tracker [10], [11]. Alternatively, deep neural networks were trained to output geometric parameters of a flexible array [12] or generate delay-and-sum ultrasound images from radiofrequency (RF) channel data without the knowledge of array geometry [13]. Recently, Omidvar *et al.* [14] proposed to optimize the average pixel brightness in a short-lag spatial coherence (SLSC) image to estimate shape variables. Limitations of these previously introduced solutions include requirements for external devices, large amounts of training data, or expensive computational calculations.

Our group previously presented a novel metric [15] that only calculates the maximum lag-one spatial coherence (mLOC) within a region of interest (ROI) surrounding a photoacoustic target to estimate flexible array curvature. This mLOC metric works by making array radius guesses and isolating the radius at whoch mLOC is maximized to determine the correct array radius. The approach is implemented with raw RF channel data without requiring supplementary tools, training datasets, or resource-intensive coherence calculations for multiple spatial lags.

We previously observed that photoacoustic source locations can influence the characteristics of mLOC when plotted as a function of array radius. In particular, unclear local maxima when plotting mLOC as a function array radius can complicate array shape estimation. Hence, more investigations into the relationships between mLOC function peaks and source locations is warranted.

The objective of the work in this paper is to investigate the effect of photoacoustic source locations on mLOC when utilized for flexible array curvature estimation. We assess the broadness of mLOC plots as a function of target location and evaluate the associated peak coherence. This work presents new insights into the effectiveness of mLOC for array shape estimation and the corresponding source locations necessary to obtain reliable estimates.

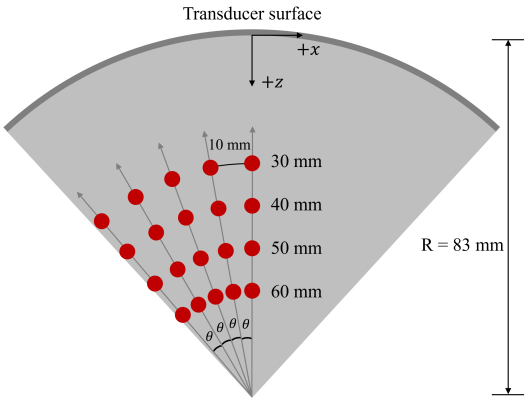

Fig. 1. A radial grid composed of 20 photoacoustic sources within the FOV of the flexible array.

II. Methods

A flexible array with 128 receive elements, 1 mm pitch, 5 MHz center frequency, and 20 MHz sampling frequency was simulated utilizing the k-Wave toolbox [16]. This flexible array was placed in a concave shape with a radius of curvature set to 83 mm. To investigate the relationship between the photoacoustic source locations and the effectiveness of mLOC, 20 acoustic sources of 0.6 mm diameter were placed in a radial grid pattern, as shown in Fig. 1. The sources were surrounded by a noiseless medium with sound speed of 1540 m/s.

In Fig. 1, the flexible array transducer surface is represented as an arc and the gray area under the arc indicates the transducer field of view (FOV), which has a sector shape. A source vector is defined as the vector from the FOV apex to the source. The azimuth is defined as the angle between the source vector and the z axis. Twenty sources were distributed along source vectors with five azimuth angles ranging from 0 to 5θ with increment of θ. In particular, four equally-spaced sources were placed along each source vector. The source distances from the sector origin were 53 mm, 43 mm, 33 mm, and 23 mm, corresponding to the shortest distances from sources to the transducer surface of 30 mm, 40 mm, 50 mm, and 60 mm, respectively. The arc length between neighbouring shallowest sources is 10 mm, resulting in θ=10.81°.

The spatial coherence of signals originating from a photoacoustic source is expected to be higher than any background signals surrounding the source. This spatial coherence calculation relies on accurate element positioning when calculating the time delays that precede spatial coherence calculations. We expect larger spatial coherence of the photoacoustic source with correct rather than incorrect element positions (assuming a correct sound speed estimate of the propagation medium). Therefore, to estimate the flexible array curvature with a known sound speed, the mLOC metric [15] was employed to calculate the maximum lag-one spatial coherence within a selected region of interested (ROI) surrounding a photoacoustic source. The normalized spatial correlation, $\hat{R}(m)$, between adjacent elements (i.e, lag $m = 1$) is calculated follows [17]:

$$\hat{R}(1) = \frac{1}{N-1}\sum_{i=1}^{N-1}\frac{\sum_{n=n_1}^{n_2} s_i(n)s_{i+1}(n)}{\sqrt{\sum_{n=n_1}^{n_2} s_i^2(n)\sum_{n=n_1}^{n_2} s_{i+1}^2(n)}} \quad (1)$$

where N is the number of receive elements in the transducer, $s_i(n)$ is the time-delayed, zero-mean photoacoustic signal received at the ith element from the nth depth (in samples). The axial correlation kernel size of $n_2 - n_1$ was fixed to be approximately one wavelength. The mLOC was calculated with a 112-element subaperture for the shallowest source locations and the full 128-element aperture for the remaining source locations (because fewer elements were needed to sample data from the shallower source and including the full aperture unnecessarily decreased the overall spatial coherence). The mLOC was then plotted as a function of array radii ranging 60 mm to 110 mm when calculating time delays. The estimated array curvature corresponded to the radius with the maximum mLOC.

To quantify the performance of our approach, the flexible array radius estimated by the maximum mLOC (i.e., the peak of the mLOC plot) obtained at each photoacoustic source location was compared with the ground truth array curvature. To investigate the effect of source locations on the most representative spatial coherence value, the maximum mLOC of each source was plotted as functions of azimuth angle and distance from the transducer surface. Considering that a smaller subaperture was used for the shallowest sources, the maximum mLOC values were compared among depths from the transducer surface ranging 40 mm to 60 mm. In addition, as the effectiveness of mLOC also depends on the narrowness of the peak, we define a new normalized full-width at half-prominence (nFWHP) metric to measure the shape of the mLOC plot:

$$\text{nFWHP} = \frac{\text{FWHP}}{\text{prominence}} \quad (2)$$

where prominence defines the relative height of a peak from its baseline and the full-width at half-prominence (FWHP) measures the width of the mLOC peak at half of the prominence value. The smaller the nFWHP, the steeper the curve surrounding the mLOC peak. At a specific distance from the transducer surface, the difference in nFWHP between any source and a source located at a 0° azimuth angle is defined as ΔnFWHP. Given that the channel signals associated with sources located at a 4θ azimuth angle were not fully visible within the flexible array FOV, our nFWHP results are only reported for sources located within 0-3θ azimuth angles.

III. Results and Discussion

Fig. 2 shows the maximum mLOC as functions of the azimuth angles of source vectors (Fig. 2(a)) and the minimum distance between sources and the flexible array surface (Fig. 2(b)). In both cases, the maximum mLOC increases with source depth, regardless of distance from the transducer center. Therefore, photoacoustic sources that are located closer to the

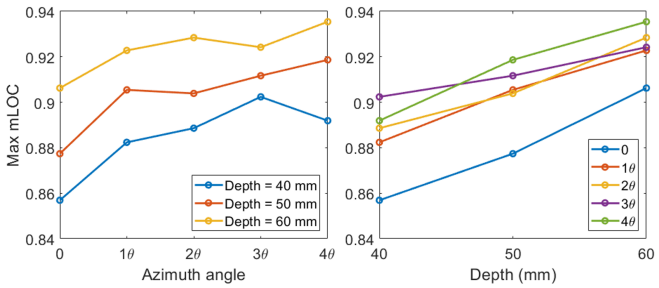

Fig. 2. The maximum mLOC as a function of (a) azimuth angles of source vectors and (b) shortest distances between sources and the transducer surface.

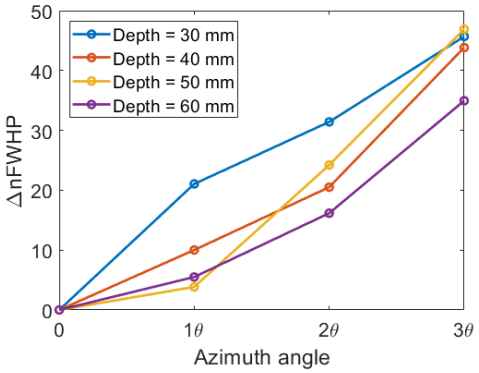

Fig. 3. The relationship between the ΔnFWHP of mLOC plots and the azimuth angle of source vectors.

center of the transducer FOV apex produce larger maximum mLOC values.

Fig. 3 shows the ΔnFWHP of mLOC plots as a function of azimuth angles between source vectors and the flexible array transducer center. Despite different receive apertures (i.e., 112 elements for the 30 mm source depth and 128 elements for the 40-60 mm source depths), ΔnFWHP increases as the azimuth angle increases, indicating that sources located closer to the transducer center have sharper mLOC peaks. These sharper peaks provide more reliable array curvature estimations. This enhanced reliability is expected to enhance the effectiveness of mLOC metric when using the corresponding information about the estimated array shape to determine beamformer time delay calculations with experimental data.

Table I summarizes flexible array curvatures estimated by mLOC peak values at the 20 photoacoustic source locations. The estimated array radius varies from 81 mm to 85 mm, resulting in 97.59%-100% accuracy when compared to the ground truth curvature, regardless of target locations in this noise-free environment.

IV. Conclusion

This work is the first to preliminarily investigate the effectiveness of the mLOC metric when applied to flexible array curvature estimation. A grid of 20 simulated photoacoustic sources was designed within the FOV of a flexible array placed in a concave shape. With the estimated array curvature,

TABLE I
FLEXIBLE ARRAY CURVATURES ESTIMATED BY MLOC

Depth	**0**	**1θ**	**2θ**	**3θ**	**4θ**
30 mm	85 mm	85 mm	83 mm	82 mm	83 mm
40 mm	84 mm	81 mm	81 mm	81 mm	84 mm
50 mm	84 mm	82 mm	82 mm	82 mm	83 mm
60 mm	84 mm	82 mm	83 mm	85 mm	84 mm

signals from sources located closer to the transducer FOV apex demonstrated greater coherence. This greater coherence is expected to translate to more distinguishable targets in photoacoustic images. The proposed nFWHP measurement provided additional quantitative insights into the broadness of the mLOC plot, demonstrating that sources located closer to the transducer center produced steeper mLOC peaks, leading to more reliable flexible transducer transducer curvature estimations. Although mLOC maintained an accuracy of 97.59%-100% when estimating array radius with our simulated results, which were implemented in a noise-free environment, these results nonetheless provide insights into ideal locations for source placement when applying mLOC to experimental data.

Acknowledgements

This work is supported by NSF SCH Award IIS 2014088 and NIH R01 EB032960.

References

[1] L. Zhang, W. Du, J.-H. Kim, C.-C. Yu, and C. Dagdeviren, "An emerging era: conformable ultrasound electronics," *Advanced Materials*, vol. 36, no. 8, p. 2307664, 2024.

[2] M. A. L. Bell, "Photoacoustic imaging for surgical guidance: principles, applications, and outlook," *Journal of Applied Physics*, vol. 128, no. 6, p. 060904, 2020.

[3] J. Zhang, A. Wiacek, Z. Feng, K. Ding, and M. A. L. Bell, "Flexible array transducer for photoacoustic-guided interventions: phantom and ex vivo demonstrations," *Biomedical Optics Express*, vol. 14, no. 8, pp. 4349–4368, 2023.

[4] J. Zhang, A. Wiacek, E. González, Z. Feng, K. Ding, and M. A. L. Bell, "A flexible array transducer for photoacoustic-guided surgery," in *Proceedings of the IEEE International Ultrasonics Symposium (IUS)*, pp. 1–4, IEEE, 2022.

[5] J. E. Aldrich, "Basic physics of ultrasound imaging," *Critical care medicine*, vol. 35, no. 5, pp. S131–S137, 2007.

[6] J. Zhang, A. Wiacek, Z. Feng, K. Ding, and M. A. L. Bell, "Comparison of flexible array with laparoscopic transducer for photoacoustic-guided surgery," in *Photons Plus Ultrasound: Imaging and Sensing*, vol. 12379, pp. 205–212, SPIE, 2023.

[7] T. Noda, N. Tomii, K. Nakagawa, T. Azuma, and I. Sakuma, "Shape estimation algorithm for ultrasound imaging by flexible array transducer," *IEEE Transactions on Ultrasonics, Ferroelectrics, and Frequency Control*, vol. 67, no. 11, pp. 2345–2353, 2020.

[8] C. J. Lane, "The inspection of curved components using flexible ultrasonic arrays and shape sensing fibres," *Case Studies in Nondestructive Testing and Evaluation*, vol. 1, pp. 13–18, 2014.

[9] V. Pashaei, P. Dehghanzadeh, G. Enwia, M. Bayat, S. J. Majerus, and S. Mandal, "Flexible body-conformal ultrasound patches for image-guided neuromodulation," *IEEE transactions on biomedical circuits and systems*, vol. 14, no. 2, pp. 305–318, 2019.

[10] D. China, Z. Feng, H. Hooshangnejad, D. Sforza, P. Vagdargi, M. A. L. Bell, A. Uneri, A. Sisniega, and K. Ding, "Flex: Flexible transducer with external tracking for ultrasound imaging with patient-specific geometry estimation," *IEEE Transactions on Biomedical Engineering*, 2023.

[11] X. Huang, H. Hooshangnejad, D. China, Z. Feng, J. Lee, M. A. L. Bell, and K. Ding, "Ultrasound imaging with flexible array transducer for pancreatic cancer radiation therapy," *Cancers*, vol. 15, no. 13, p. 3294, 2023.

[12] T. Noda, T. Azuma, Y. Ohtake, I. Sakuma, and N. Tomii, "Ultrasound imaging with a flexible probe based on element array geometry estimation using deep neural network," *IEEE Transactions on Ultrasonics, Ferroelectrics, and Frequency Control*, vol. 69, no. 12, pp. 3232–3242, 2022.

[13] X. Huang, M. A. L. Bell, and K. Ding, "Deep learning for ultrasound beamforming in flexible array transducer," *IEEE Transactions on Medical Imaging*, vol. 40, no. 11, pp. 3178–3189, 2021.

[14] A. Omidvar, R. Rohling, E. Cretu, M. Cresswell, and A. J. Hodgson, "Shape estimation of flexible ultrasound arrays using spatial coherence: A preliminary study," *Ultrasonics*, vol. 136, p. 107171, 2024.

[15] J. Zhang, K. Ding, and M. A. L. Bell, "Flexible array curvature and sound speed estimations with a maximum spatial lag-one coherence metric," in *Photons Plus Ultrasound: Imaging and Sensing 2024*, vol. 12842, pp. 309–314, SPIE, 2024.

[16] B. E. Treeby and B. T. Cox, "k-wave: Matlab toolbox for the simulation and reconstruction of photoacoustic wave fields," *Journal of biomedical optics*, vol. 15, no. 2, pp. 021314–021314, 2010.

[17] M. A. Lediju, G. E. Trahey, B. C. Byram, and J. J. Dahl, "Short-lag spatial coherence of backscattered echoes: Imaging characteristics," *IEEE Transactions on Ultrasonics, Ferroelectrics, and Frequency Control*, vol. 58, no. 7, pp. 1377–1388, 2011.